International Journal of Fracture **128:** 1–15, 2004.
© 2004 *Kluwer Academic Publishers. Printed in the Netherlands.*

Characteristic dimensions and the micro-mechanisms of fracture and fatigue in 'nano' and 'bio' materials

R.O. RITCHIE*, J.J. KRUZIC, C.L. MUHLSTEIN[1], R.K. NALLA and E.A. STACH
Materials Sciences Division, Lawrence Berkeley National Laboratory, and Department of Materials Science and Engineering, University of California, Berkeley, CA, USA
**Author for correspondence (E-mail: roritchie@lbl.gov; Phone: 510-486-5798)*

Abstract. The behavior of small-volume (so-called 'nano') structures, where size-scales are comparable with microstructural dimensions, and biological/bio-implantable materials, which invariably display a hierarchy of structural dimensions, is currently much in vogue in materials science. One aspect of this field, which to date has received only limited attention, is the fracture and fatigue properties of these materials. In this paper, we examine two topics in this area, namely the premature fatigue failure of silicon-based micron-scale structures for microelectromechanical systems (MEMS), and the fracture properties of mineralized tissue, specifically human bone.

Key words: Bone, fatigue, fracture toughness, MEMS, polysilicon, thin films.

1. Introduction

Materials scientists currently live in a world dominated by 'buzz words' that define what is currently in favor and hence what is fundable and worthy of study. At present, two of the most important words are 'nano' and 'bio', which respectively describe the areas of nanostructured materials/small-volume structures and biological/bio-implantable materials. With respect to the problems of fracture and fatigue, however, both areas lack the sound understanding that we typically associate with traditional engineering materials and structures, and yet they clearly offer 'fruitful ground' for fascinating new studies. This presentation focuses on two such topics, namely (i) the failure of 'small-volume' structures for microelectromechanical systems (MEMS), specifically involving the high-cycle fatigue of micron-scale thin films of silicon, and (ii) the fatigue and fracture toughness properties of the mineralized tissues, specifically human bone, in simulated physiological environments.

With respect to the high-cycle fatigue of thin-film silicon, micron-scale structures of mono- and polycrystalline silicon have been found to be vulnerable to degradation by fatigue in ambient air and to fail after lives in excess of 10^{11} cycles at stresses as low as half the (single-cycle) fracture strength. Indeed, although bulk silicon is ostensibly immune to cyclic fatigue and subcritical crack growth, micron-scale films of silicon actually display 'metal-like' stress-life (*S/N*) fatigue behavior. Our experiments, however, have clarified the origin of this fatigue susceptibility of thin-film silicon. *S/N* fatigue testing, transmission electron microscopy, infrared microscopy and numerical models have been used to establish that the mechanism of such failure involves the sequential oxidation and environmentally-assisted crack growth of

[1]Current address: The Pennsylvania State University, University Park, PA 16802, USA.

the oxide layer, a process that is termed 'reaction-layer fatigue'. Only thin film/small volume silicon structures are prone to such failures, as the critical crack size for catastrophic failure of the entire structure can be exceeded by a nano-scale crack solely within the oxide layer. Methods to reduce this susceptibility, through the use of monolayer coatings, are described.

Turning to the fracture properties of mineralized tissue such as human bone, although there is substantial clinical interest in its fracture resistance, little mechanistic information is available on how such materials derive their toughness and how they are specifically affected by fatigue. For example, the critical fracture event in human bone is widely believed to be locally strain-controlled, although no direct evidence has ever been offered to support this belief. In this paper, *in vitro* experiments are described involving a novel double-notched four-point bend geometry, which is designed to discern whether the onset of fracture is stress- or strain-controlled. Such experiments are further used to examine the interaction of cracks with the microstructure in bone in order to characterize the salient mechanisms of toughening. It is found that the precursor fracture events are consistent with a strain-based mechanism, and that toughening is developed through a variety of extrinsic mechanisms, including crack bridging (from collagen fibrils and uncracked ligaments) and diffuse microcracking, over a variety of length-scales.

2. Fatigue of 'small volumes'

Silicon-based structural films remain the dominant material for MEMS because the micromachining technologies are readily adaptable from the microelectronics industry and are compatible with fabrication strategies for actuation and control integrated circuits. However, the long-term durability of MEMS may be compromised by a susceptibility of thin-film silicon to premature failure by fatigue (Connally and Brown, 1992; Brown et al., 1997; 2002b; Komai et al., 1998; Kahn et al., 1999a; Van Arsdell and Brown, 1999; Allameh et al., 2000; Muhlstein et al., 2001a, 2001b, 2002a).

In ductile materials, fatigue is attributed to cyclic plasticity involving dislocation motion that causes alternating blunting and resharpening of a pre-existing crack tip as it advances (Ritchie, 1999; Suresh, 1998). In brittle materials where dislocation mobility is restricted, fatigue conversely occurs by cycle-dependent degradation of the (extrinsic) toughness of the material in the wake of the crack tip (Ritchie, 1999). As silicon is a brittle material (no dislocation activity is generally observed below ~ 500 °C) that displays little evidence of extrinsic toughening (Kahn et al., 1999a) or susceptibility to environmental cracking (Lawn et al., 1981), it should not fatigue at room temperature. Indeed, there is no evidence that bulk silicon is prone to fatigue failure. However, cyclically-stressed silicon films at the micron-scale are known to fail in room air at stresses well below their fracture strength (Connally and Brown, 1992; Brown et al., 1997; 2002b; Komai et al., 1998; Kahn et al., 1999a; Van Arsdell and Brown, 1999; Allameh et al., 2000; Muhlstein et al., 2001a, b, 2002a).

Although first reported a decade ago (Connally and Brown, 1992), the mechanistic origins of such micron-scale silicon fatigue have remained elusive. In this paper, experimental evidence is shown that the cracking processes associated with the fatigue of thin-film silicon are confined to the nanoscale oxide layer; further, we present a mechanism for such behavior involving sequential oxidation and moisture-assisted cracking in this amorphous layer. Additionally, a method for suppressing the cyclic fatigue of silicon is suggested through the use of alkene-based, monolayer coatings that totally inhibit the formation of the native oxide layer.

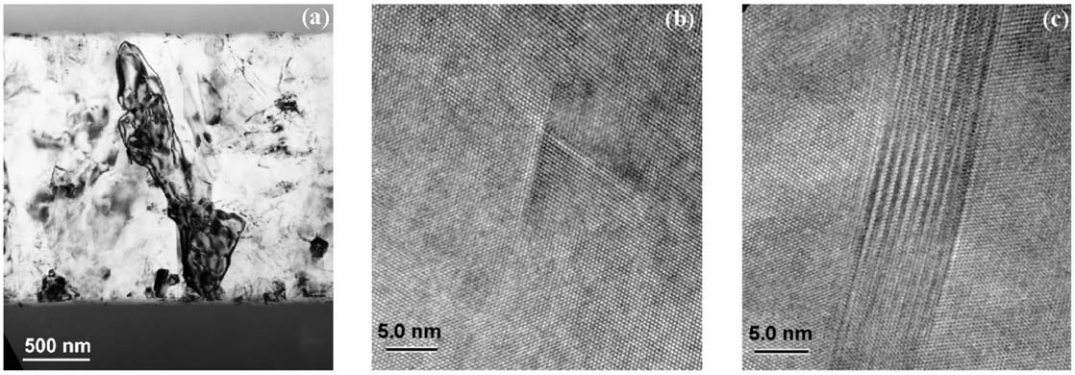

Figure 1. Microstructure of the 2 μm thick polysilicon films: (a) cross sectional TEM image, (b) Lomer-Cottrell lock, and (c) microtwins.

2.1. MICROSTRUCTURE OF MICRON-SCALE SILICON FILMS

The thin films examined were low-pressure chemical vapor deposited (LPCVD) n^+-type polycrystalline silicon, fabricated as 2-μm thick films by using the MCNC/Cronos MUMPs^{TM} process. Wafer curvature measurements indicated a compressive residual stress in the films of ~ -9 MPa. Secondary ion mass spectroscopy (SIMS) analysis revealed the presence of $\sim 2 \times 10^{18\ \text{atoms}}/\text{cm}^3$ hydrogen, $1 \times 10^{18\text{atoms}}/\text{cm}^3$ oxygen, and $6 \times 10^{17\text{atoms}}/\text{cm}^3$ carbon (Connally and Brown, 1980); in addition, $1 \times 10^{19\text{atoms}}/\text{cm}^3$ of phosphorous were detected from the phosphosilicate glass used for doping. The films, which were representative of those used throughout micromachining and MEMS research and production, had a Young's modulus of 163 GPa and a Poisson's ratio of 0.23. Fracture strengths typically ranged from 3 to 5 GPa, depending on loading condition, specimen size, and test technique, with a fracture toughness, K_c, of ~ 1 MPa$\sqrt{\text{m}}$ (Kahn et al., 1999b).

The film microstructures had an equiaxed grain morphology (grain size of ~ 100 nm), with no strong texture, no segregation of O, C, P or N, or precipitation of secondary species. Diffraction contrast imaging using transmission electron microscopy (TEM) revealed several types of lattice defects, including microtwins, stacking faults and Lomer-Cottrell dislocation locks (Figure 1) (Muhlstein et al., 2002b).

2.2. MICRON-SCALE FATIGUE TESTING

Fatigue life as a function of applied stress was determined by using a notched cantilever-beam specimen within a micron-scale 'on-chip' fatigue characterization structure, as shown in Figure 2 (Muhlstein et al., 2001a, b). Polysilicon samples were prepared by removing the sacrificial oxide layer in 49% HF for $2\frac{1}{2} - 3$ min, drying at 110 °C in air, and mounting in ceramic electronic packages. The notched beam specimen (~ 40 μm long, 19.5 μm wide, and 2 μm thick, with a 13 μm deep, 1 μm radiused notch), was attached to a large, perforated plate that served as a resonant mass. The mass and beam were electrostatically forced to resonate and the resulting motion was measured capacitively. This generated fully-reversed, constant-amplitude, sinusoidal stresses at the notch, i.e., a load ratio of $R = -1$, that were controlled to better than 1% precision. Specimen were cycled to failure at resonance with a frequency of ~ 40 kHz in ambient air (~ 25 °C, 30–50% relative humidity) at stress amplitudes ranging from 2 to 4 GPa, using the control scheme described by Muhlstein et al., (2001a, b).

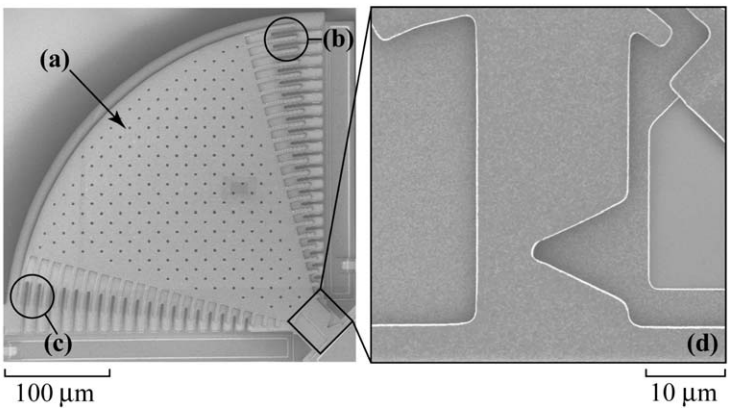

Figure 2. Scanning electron micrographs (SEM) of the fatigue test structure, showing the (a) mass, (b) comb drive actuator, (c) capacitive displacement sensor, and (d) notched cantilever-beam specimen.

The specimen compliance, computed from change in the natural frequency of the system (Muhlstein et al., 2001b, 2004), was monitored *in situ* to evaluate the evolution of damage in the sample from cracking and oxide formation. Experiments using an unnotched specimen have been used to demonstrate that changes in resonant frequency are a result of such damage and are not due to variations in temperature, relative humidity or accumulation of debris (Van Arsdell and Brown, 1999). The relationship between stresses in the vicinity of the notch and its dynamic response was determined with finite-element modeling. Such methods were also used to evaluate the natural frequency, compliance, crack length, and stress-intensity factor, K, for structures containing cracks. The numerical models were constructed with a commercial software package (ANSYS v 5.7) (Muhlstein et al., 2004).

2.3. Micron-scale stress-life fatigue

Stress-life (*S/N*) data for the micron-scale polysilicon films are shown in Figure 3a, based on a total of 28 specimens tested in room air (Muhlstein et al., 2001b). The silicon films can be seen to display 'metal-like' *S/N* behavior, with an endurance strength at 10^9–10^{10} cycles of roughly half the (single-cycle) fracture strength. Similar behavior has been seen in 20-μm thick films of single-crystal silicon cycled under identical conditions (Muhlstein et al., 2001a). The change in resonant frequency of the specimens was monitored during testing to provide a measure of the specimen compliance. The frequency decreased (by up to 50 Hz in the long-life tests) before eventual specimen failure at the notch; indeed, by using plane-stress finite element modal analyses with ANSYS (Muhlstein et al., 2001b, 2004), this was related to the stable growth of a crack (Figure 3b). This analysis implies cracking occurring on length scales commensurate with the oxide thickness; indeed, estimates of the crack length, plotted in Figure 3b, reveal crack sizes less than 50 nm throughout the entire test.

SEM and TEM of failed specimens established that overload fracture in the films occurred by transgranular cleavage. Although SEM studies were inconclusive in discerning differences between these and the fatigue fractures, this was clearly evident in high-voltage ($\sim$ 1 MeV) TEM. Examination of fatigue and untested control samples revealed a stark difference in the oxide at the notch root. In control samples, a $\sim$ 30 nm thick layer of oxide was uniformly distributed over the sample surfaces (including the notch); in the fatigue samples, however, the oxide layer at the notch was up to a factor of three thicker (Figure 4a).

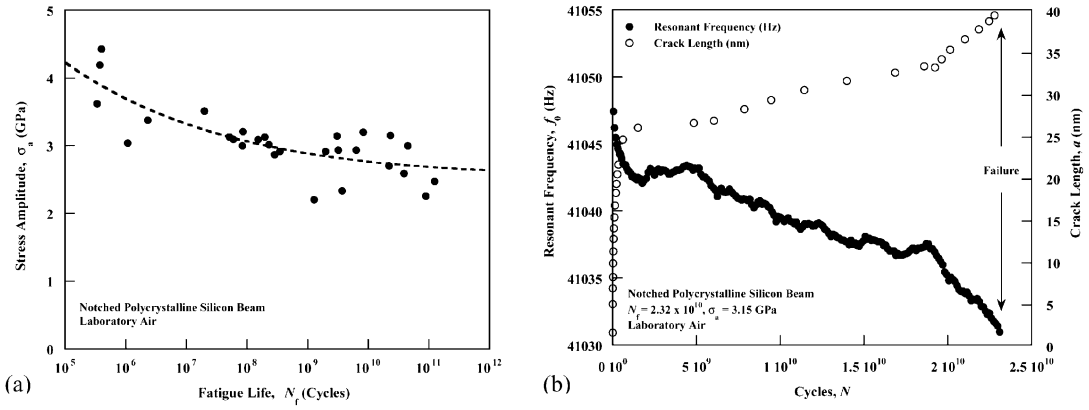

Figure 3. (a) Stress-life curves for 2 μm-thick polysilicon at 40 kHz in moist air at $R = -1$. (b) *In situ* damage accumulation as a decrease in resonant frequency, f_{crack}, with time, with corresponding calculated increase in crack length, a.

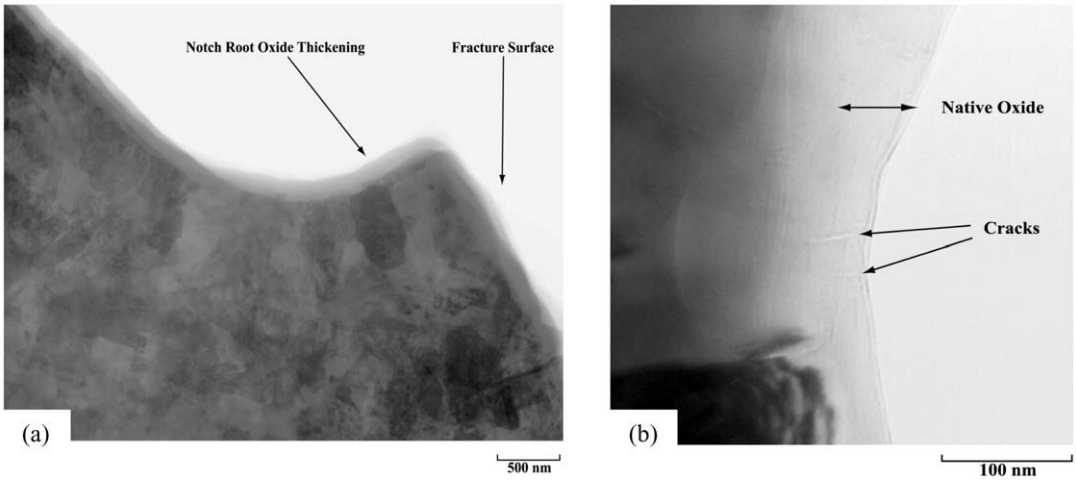

Figure 4. TEM images of the notch region in an unthinned polysilicon test sample, showing (a) enhanced oxidation at the notch root after fatigue cycling, and (b) $\sim$ 50 nm long stable cracks in the oxide layer formed during cyclic loading.

As *in situ*, high-resolution infrared imaging of the fatigue characterization structure revealed no changes in temperature greater than 1 °C at the notch root during testing, the enhanced notch-root oxidation appeared to be mechanical in origin (Muhlstein et al., 2002a, b).

The precise nature of this effect is presently unclear, but may be related to such processes as stress-assisted diffusion and cracking within the notch oxide layer, which permits the further ingress of moisture and continued oxidation in this region (e.g. Fargeix and Ghibaudo, 1984). Despite uncertainty in the origin of this layer, its role in thin-film silicon fatigue is far clearer. By interrupting fatigue specimens prior to failure and examining them with TEM, several small growing cracks (on the order of tens of nanometers in length) were observed within the oxide at the notch root (Figure 4b). The size of these cracks was consistent with the compliance change predicted by finite-element modeling. Such cracking in the oxide layer is considered to be moisture-induced. Since the toughness of the SiO_2 ($K_c \sim 0.8$ MPa$\sqrt{\text{m}}$)

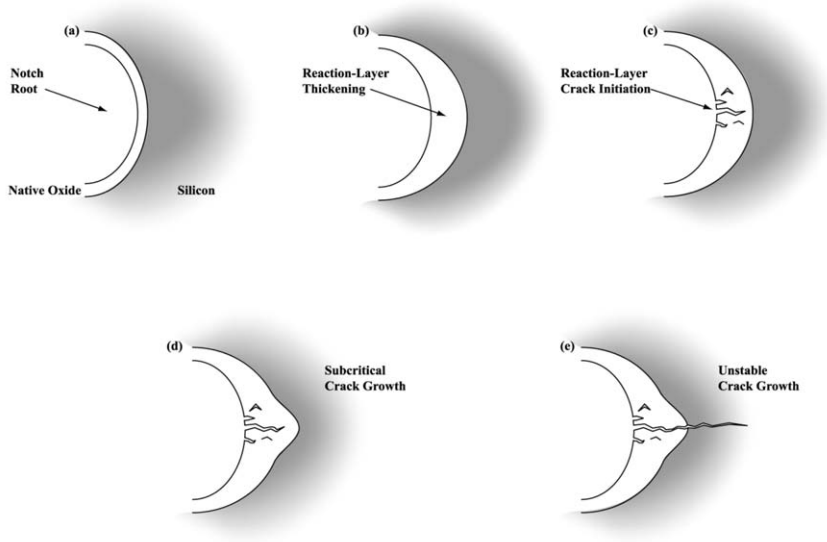

Figure 5. Schematic illustration of the 'reaction-layer fatigue' mechanism at the notch of the polycrystalline silicon cantilever beam.

is comparable to that of silicon ($K_c \sim 1$ MPa$\sqrt{}$m), the oxide should not crack prematurely. However, unlike silicon, amorphous SiO_2 is susceptible to environmentally-assisted cracking in moisture; indeed, the threshold stress intensity, K_{scc}, for such cracking is much less than K_c, i.e., $K_{scc} \sim 0.25$ MPa$\sqrt{}$m, in contrast to silicon where $K_{scc} \approx K_c$ (Lawn et al., 1981). Since no phase transformations or dislocation activity were detected, the fatigue of Si films in ambient air was deemed to be associated with environmentally-assisted cracking in the oxide layer that has been thickened under cyclic loading (Figure 5).

In situ measurements of the natural frequency during the fatigue test were used to determine the crack length and hence the crack-driving force at failure; this provides a measure of the fracture toughness, which was computed to be ~ 0.85 MPa$\sqrt{}$m, consistent with that of the native oxide (Muhlstein et al., 2004). However, it is important to note the relationship between the critical crack size at final failure, a_c, where $K = K_c$, and the thickness, h_o, of the SiO_2 layer. If critical crack sizes are estimated for the range of applied stresses of $\sigma_a \sim 2$ to 4 GPa which caused failure in the present films after 10^5 to 10^{11} cycles (Figure 6), it is apparent that the critical crack sizes are less than 50 nm, i.e., comparable to the observed oxide layer thicknesses (i.e., $a_c \leqslant h_o$). This indicates that the entire fatigue-crack initiation and propagation process and the onset of catastrophic (overload) failure all occur within the oxide layer.

2.4. 'REACTION-LAYER' FATIGUE

The cyclic fatigue of brittle materials is caused by the degradation of extrinsic toughening mechanisms in the crack wake (Ritchie, 1999). Such toughening arises from crack-tip shielding, which in brittle ceramic materials generally results from mechanisms such as grain bridging. Under cyclic loading, frictional wear in the sliding grain boundaries can lead to a decay in the bridging stresses (Lathabai, 1991, Dauskardt, 1993; Ritchie, 1999). The fatigue of brittle materials is thus often associated with intergranular failure. When such materials fail

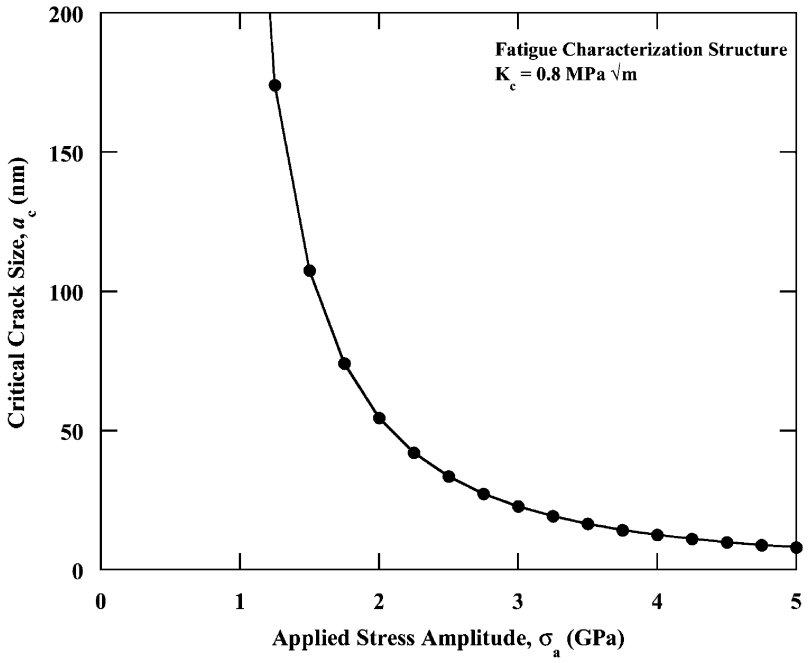

Figure 6. Computed estimates of the critical crack size, a_c, as a function of the applied stress amplitude, σ_a, in the fatigue specimens. Critical crack sizes for the stress amplitudes used ($\sigma_a \sim 2$ to 4 GPa) are less than ~ 50 nm, indicating that the onset of final failure of the structure occurs within the oxide layer.

transgranularly, there is little susceptibility to fatigue. Since polysilicon fails transgranularly with little evidence of extrinsic toughening, it would not be expected to be prone to fatigue. Similarly, below $\sim$ 500 °C, there is no evidence of mobile dislocation activity (Lawn et al., 1980), which could cause fatigue failure as in a ductile material.

However, the fatigue susceptibility of micron-scale thin-film silicon is associated with a conceptually different mechanism, that of sequential mechanically-induced oxidation and environmentally-assisted cracking of the surface layer of oxide that forms upon reaction with the atmosphere (reaction-layer fatigue) (Figure 5). This mechanism was observed experimentally as a continuous decrease in the specimen stiffness during fatigue loading (Muhlstein, 2001b) and was visualized directly with TEM. The native oxide, which initially forms on the exposed silicon surface, thickens in high stress regions during fatigue loading and becomes the site for moisture-induced cracks that grow stably in the oxide layer. The process repeats itself until a critical crack size is reached, whereupon the silicon itself fractures catastrophically. The rate-dependence of thin-film silicon fatigue is thus dictated by the cycle-dependent oxide thickening process and the time-dependent moisture-assisted subcritical crack growth in this oxide layer, all processes that occur at nanoscale dimensions.

This mechanism provides an explanation as to why micron-scale silicon is prone to fatigue failure, even though bulk silicon is not. This is because cracking in the nano-scale oxide film would have a negligible effect on a macroscopic sample of silicon under load, since crack sizes in the oxide could never reach critical size. In contrast, with thin films where the surface-to-volume ratio is far larger such that the oxide layer represents a large proportion of the sample, cracks within the oxide are readily able to exceed critical size and thus can cause failure of the entire silicon component.

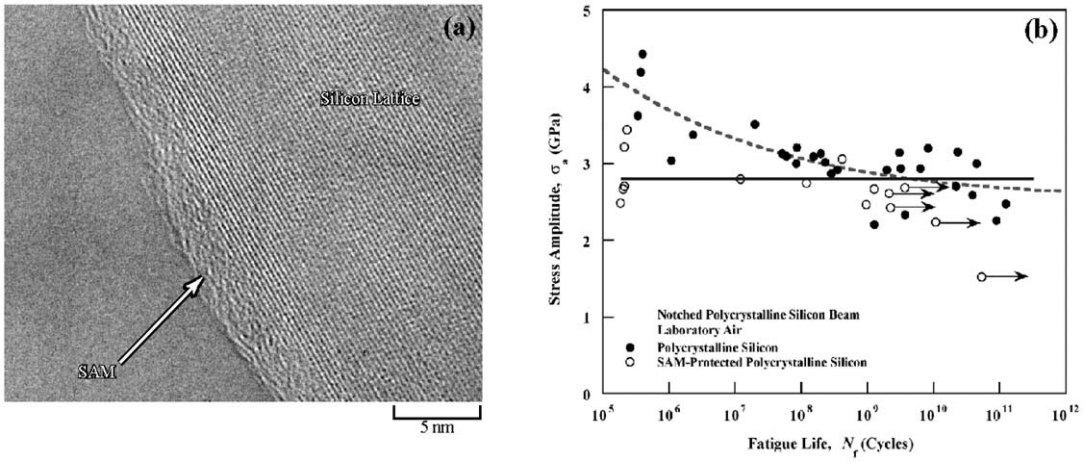

Figure 7. (a) TEM image showing a 1-octadescene self-assembled monolayer (SAM) coating the root of the polysilicon notch; the absence of the oxide is shown by the lattice fringes of the silicon visible under the ∼ 3 nm layer. (b) *S/N* curves showing the reduced susceptibility of such SAM-coated polysilicon films to fatigue failure.

An obvious test of this mechanism is to fatigue in an environment where the oxide cannot form. This was achieved through the use of coatings to suppress the formation of the native oxide. Accordingly, specific specimens were coated after HF release with a hydrophobic monolayer of alkene-based 1-octadecene ($C_{16}H_{33}CH = CH_2$), which bonds directly to the H-terminated Si atoms on the surface such that no oxide can form (Figure 7a) (Ashurst et al., 2001). Thirteen specimens were then tested to failure and five were interrupted prior to failure for examination in the TEM. Fatigue lives varied from ∼ 7.5 sec to 25 days (3×10^5 to 8.9×10^{10} cycles) for stress amplitudes ranging from ∼ 1.4 to 3.3 GPa at a load ratio R of -1 (Figure 7b). In contrast to the specimens without the coating, the behavior is reminiscent of bulk brittle materials. High-voltage TEM of protected specimens after testing shows that the failure is associated with local oxidation at the notch root while the 1-octadecene monolayer remains intact on the rest of the specimen (Figure 8). These results on such coated films, where the oxide cannot form, clearly show fatigue lifetimes that are far less affected by cyclic stresses (Figure 7b), thereby providing strong support for the proposed reaction-layer mechanism of thin-film silicon fatigue.

3. Fracture of biomaterials

Similar to the problem of small volume structures, biomaterials also represent an area where there is only limited understanding of mechanical behavior and its mechanistic origins. A mechanistic understanding of fracture in human bone, for example, is critical to predicting fracture risk associated with age and disease. Despite extensive work, a mechanistic framework for describing how the microstructure affects the failure of bone is lacking. Though micromechanical models incorporating local failure criteria have been developed for metallic and ceramic materials (Ritchie et al., 1973, 1979), few such models exist for biological materials. In fact, there is no proof to support the widely held belief that fracture in bone is locally strain-controlled (Yeh and Keaveny, 2001; Keyak and Rossi, 2000). Below, a series of experiments is described to obtain such evidence using a double-notch-bend geometry designed to shed light on the nature of the critical failure events in bone. In addition, how

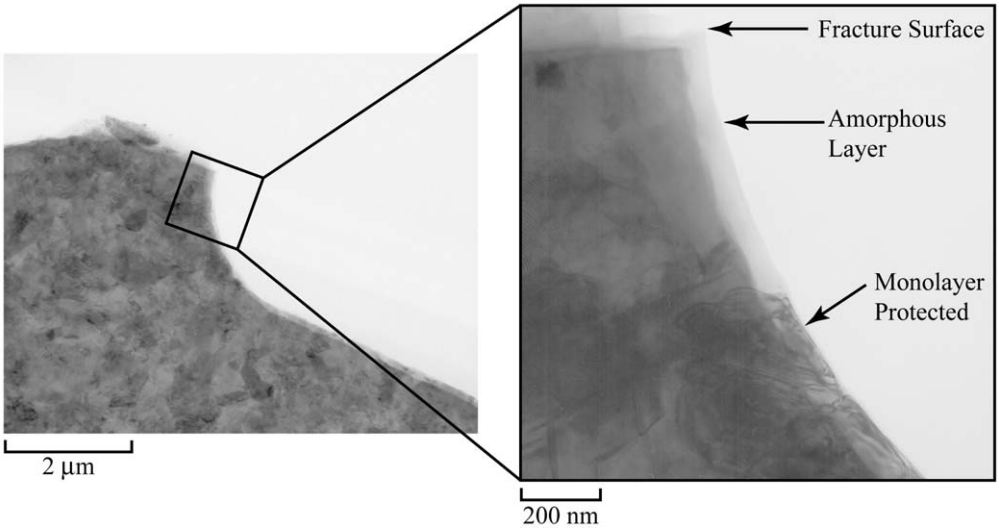

Figure 8. High-voltage transmission electron microscopy (HVTEM) image of the notch region of a 1-octadecene-protected polysilicon specimen that failed under fatigue loading conditions.

the propagating crack interacts with the many dimensional levels of bone microstructure is examined to provide some mechanistic understanding of fracture and to define how properties vary with orientation.

3.1. Microstructure of human bone

Human bone has a complex hierarchical microstructure that can be considered at many dimensional scales (Rho, et al., 1998; Weiner and Wagner, 1998). At the shortest length-scale, it is composed of type-I collagen fibers (up to 15 μm in length, 50–70 nm in diameter) bound and impregnated with carbonated apatite nanocrystals (tens of nm in length and width, 2–3 nm in thickness) (Rho, et al., 1998). These mineralized collagen fibers are further organized at a microstructural length-scale into a lamellar structure with roughly orthogonal orientations of adjacent lamellae (3–7 μm thick) (Weiner and Wagner, 1998). Permeating this lamellar structure are the secondary osteons (up to 200–300 μm diameter): large vascular channels (up to 50–90 μm diameter) oriented roughly in the growth direction of the bone and surrounded by circumferential lamellar rings. The difficulty in understanding the mechanisms of fracture in bone lies in determining the relative importance of these microstructural hierarchies on crack initiation, subsequent crack propagation and consequent unstable fracture, and in separating their effects on the critical fracture events.

Double-notch, four-point bend testing

A vital distinction in the definition of the local (precursor) fracture events that cause macroscopic failure is whether they are locally *stress-* or *strain-controlled*. Brittle fracture is invariably stress-controlled, for example in structural steels at low temperatures, where cleavage fracture is instigated by the precursor cracking of carbide particles or inclusions (Ritchie et al., 1973, 1979). Ductile fracture, conversely, is strain-controlled, as in the same steels at higher temperatures where the fracture process involves ductile tearing between such particles or inclusions (with a significant increase in toughness) (e.g., Ritchie et al., 1979). Bone fracture

is widely regarded as strain-controlled; indeed, most theoretical descriptions of its mechanical behavior assume this to be the case (Yeh and Keaveny, 2001). However, experimental evidence for this assertion has never been obtained.

To investigate this distinction, a double-notched four-point bend test was used, consisting of a rectangular bar containing two nominally identical rounded notches (root radius $\sim$ 200 μm) subjected to four-point bending. The basis of the test is that with a rounded notch in the presence of some degree of inelasticity or yielding, although the maximum local strains are located at the root of the notch, the relaxation of stresses in the inelastic ('yielded') zone surrounding the notch results in the maximum local stresses being located some distance *ahead* of the notch, close to the elastic-inelastic interface (Griffiths and Owen, 1971) (Figure 9a). Since the two notches experience the same bending moment, when one notch breaks, the other is 'frozen' at a point immediately preceding fracture. Examination of the area in the vicinity of the unfractured notch thus reveals the nature of the *local* fracture event at the onset of failure (as indicated in the area indicated in Figure 9b '*After fracture*' illustration).

It is appreciated that 'yielding' in bone cannot be simply related to shear-driven plasticity, e.g., in metals, for which the notch-field solutions in Figure 9a were explicitly derived. Indeed, the precise nature of the inelastic constitutive behavior of bone is not known, but clearly involves diffuse microcracking damage and plasticity in the collagen fibrils, which would be sensitive to both tensile and shear stresses (somewhat akin to pressure-dependent yielding in polymers). Despite this, most theoretical models for both deformation (Zioupos et al., 1995) and fracture (Lotz et al., 1991) in bone utilize the Mises criterion, which was derived for pressure-insensitive plasticity. Our recent studies using a microcracking model for inelastic deformation have in fact shown that the notch fields for an idealized bone-like material are qualitatively identical to those for pressure-insensitive shear-driven plasticity (Nalla et al., 2004).

Results for tests in a simulated physiological environment (Hanks' Balanced Salt Solution) are shown in Figure 10, and show the unbroken notches in specimens of a cadaveric human humerus. The extremely small (< 5 μm) size of the precursor cracks that were imaged in all orientations (Figure 9c) leaves little doubt that crack initiation is *at* the notch and not ahead of it (Figure 10). Moreover, assuming a plasticity-based criterion, numerical analysis of the specimens at maximum load where the nominal elastic bending stress, σ_{nom}, at the notch was in the 40 to 100 MPa range (ratio of nominal stress to yield stress of $\sigma_{nom}/\sigma_y \sim 0.53$–$1.33$), suggests that the tensile stresses should peak well ahead of the notch (at $\sim$ 100–360 μm ahead of the notch tip, *i.e.*, at a distance of 0.5–1.2 times the notch-root radius). As absolutely no evidence of any precursor cracking was found in this region and all initial cracks were detected exactly at the notch root, our observations are consistent with fracture in bone being associated with a strain-based criterion. Similar studies with identical results have been performed for dentin, the principal constituent of human teeth (Nalla et al., 2003).

3.2. Mechanisms of fracture in bone

Insights into the mechanisms of fracture in bone and how it derives its toughness can also be obtained from these experiments. Various toughening mechanisms have been proposed for bone. At large length-scales, the generation of 'microdamage' from microcracking (small cracks of up to hundreds of micrometers in size) has been suggested as a source of toughening in bone, specifically via crack-tip shielding (Parsamian and Norman, 2001; Vashishth et al.,

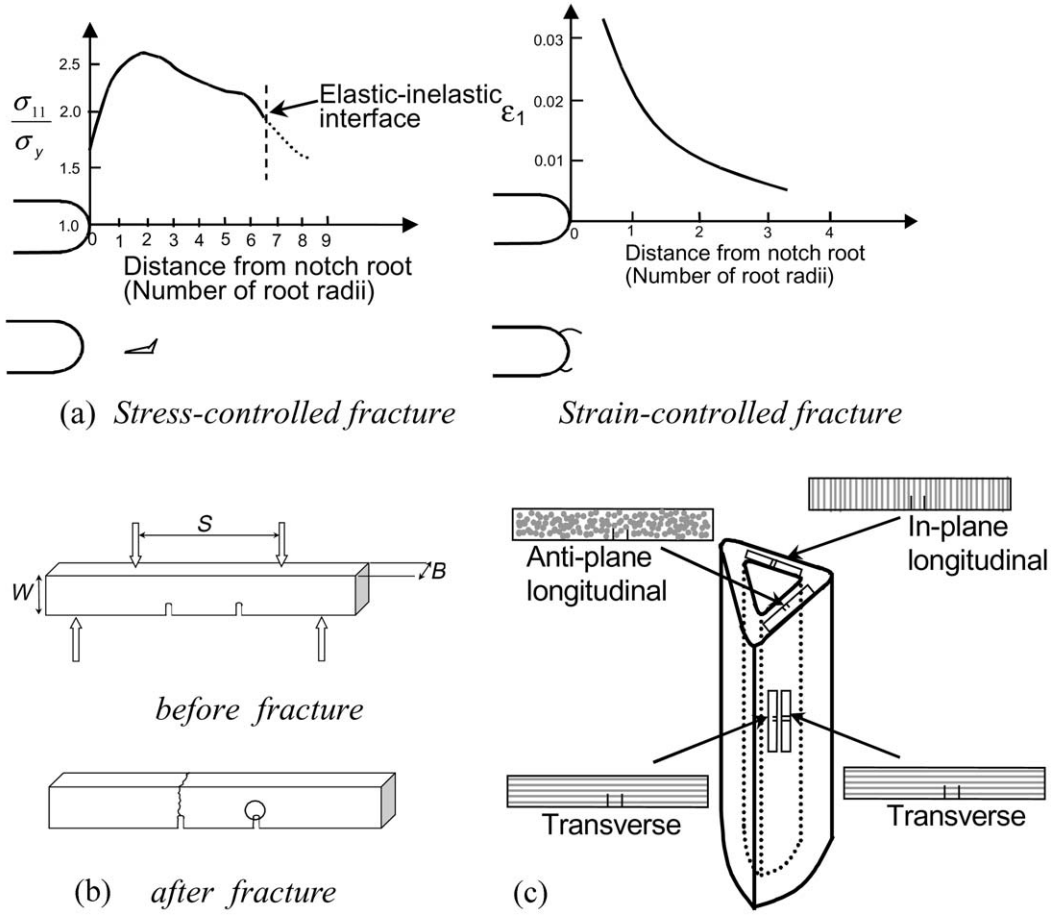

Figure 9. (a) The stress (left) and strain (right) distributions ahead of a notch, indicating that, in the presence of inelasticity, the peak stresses are *ahead* of the notch whereas the peak strains are *at* the notch. Consequently, stress-controlled fracture will initiate ahead of the notch, whereas the initial fracture event for strain-controlled fracture will be at the notch. (b) Double-notched four-point bend test. (c) Specimen orientations taken from the humerus (relative to the direction of the osteons, indicated in grey).

2000). In addition, the cement lines (at the secondary osteons boundaries) and the interlamellar boundaries are believed to provide weak interfaces to deflect the crack path and accordingly increase the toughness (Yeni and Norman, 2000). More recently, a role of collagen fibrils has been postulated (Wang et al., 2001), with fiber bridging proposed as a possible toughening mechanism (Yeni and Fyhrie, 2001). Indeed, toughening at the fibrillar level would explain the apparent correlation of toughness with collagen denaturation, which appears to weaken bone, and cross-links, which appear to increase its toughness (Burr, 2002), although it is probable that many of these mechanisms operate in concert.

Scanning electron micrographs of the fracture paths in human bone, specifically indicating how the crack interacts with the microstructure, are shown in Figure 11. Figure 11a shows a roughly 1-mm-long crack propagating out of the notch in the 'anti-plane longitudinal' orientation, i.e., the plane of the crack and the crack front are nominally parallel to the long axis of the osteons. It is apparent that at this scale of observation, the most recognizable features of the microstructure, the Haversian canals with their concentric lamellar rings, do

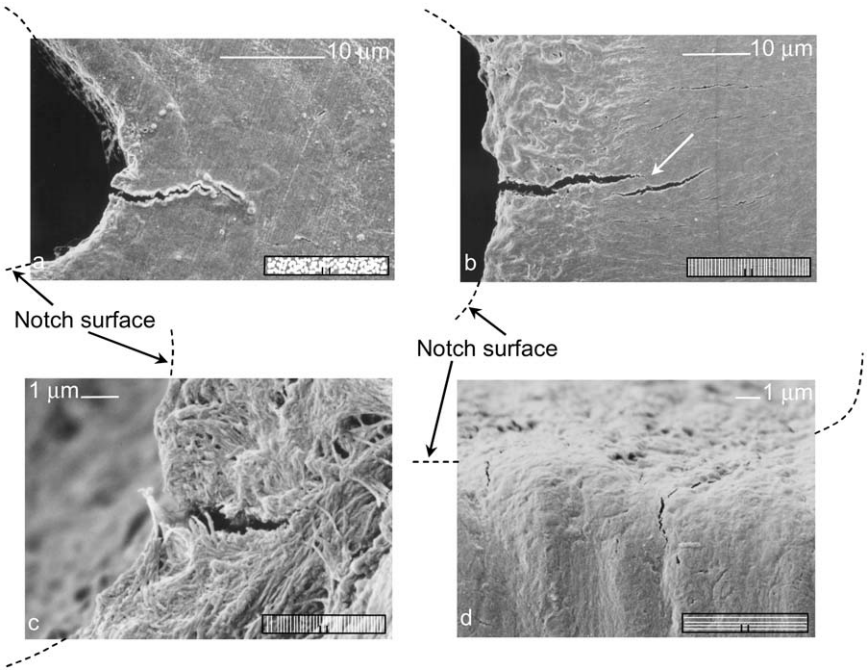

Figure 10. SEM micrographs of the area near the unbroken notch: (a) A crack emanating directly from the notch in the 'anti-plane longitudinal' orientation. (b) Uncracked ligament bridging (indicated by white arrow) and microcracking for the 'in-plane longitudinal' orientation. (c) The < 5 μm size of precursor cracks shows that initiation is at the notch and not ahead of it, consistent with locally strain-controlled fracture. (d) The strong influence of microstructure leads to cracks emanating well behind the notch root in the 'transverse' orientation. Also, multiple crack initiation can be seen. The insets show the specimen orientation with respect to the direction of the osteons.

not have a major influence on the path taken by the growing crack. Investigation of the near-tip region of this crack, however, revealed evidence of so-called uncracked-ligament bridging, as indicated by the white arrow in Figure 11b. This is an extrinsic toughening mechanism involving two-dimensional uncracked regions along the crack path that can bridge the crack on opening; it is commonly seen in metal-matrix composites (Shang and Ritchie, 1989) and intermetallics such as γ-based TiAl (e.g., Campbell et al., 1999). Such uncracked-ligament bridging, however, is more prominent in the 'in-plane longitudinal' orientation, as shown by the white arrow in Figure 10b, where evidence of microcracking is also apparent near the crack. This can also lead to extrinsic toughening through its effect in creating dilation and reducing the modulus in the region surrounding the crack. For the 'anti-plane longitudinal' orientation, a third mechanism of toughening in bone can be seen in Figure 11c in the form of crack bridging by the collagen fibrils.

However, for the 'transverse' specimen orientations, where the osteons run along the specimen length (Figure 9c), a much stronger influence of the underlying microstructure was observed on the crack path. Crack initiation and initial crack growth out of the notch was not in the direction normal to the maximum tensile stress, but rather in the direction of the osteons (Figure 10d), consistent with the suggestion (Yeni and Norman, 2000) that the osteonal cement lines, which are the interface between the osteonal system and the surrounding matrix, can provide a weak path for the propagation of the crack. The resulting large out-of-plane crack deflections can lead to substantial toughening (as estimated below) and must be considered

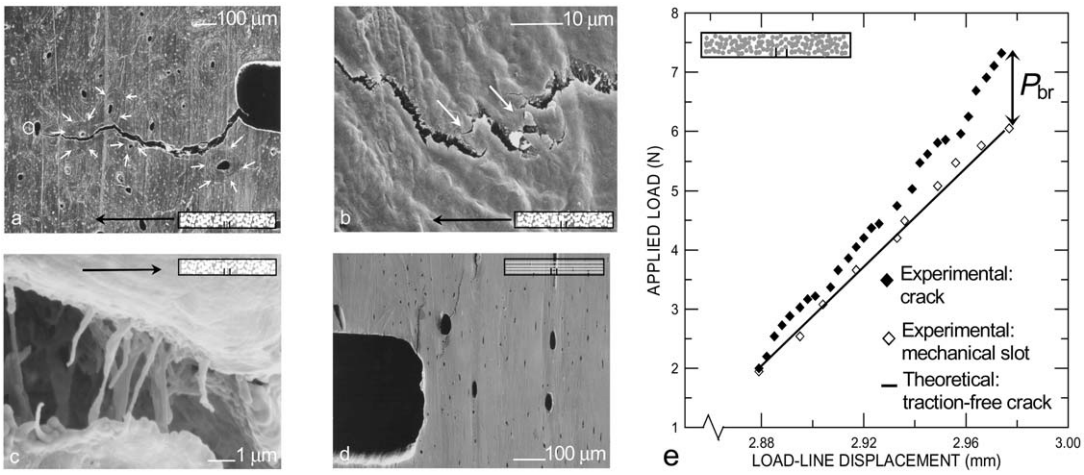

Figure 11. SEM micrographs illustrating toughening mechanisms in bone through interactions between the crack and the microstructure: (a) For a crack emanating from the notch in the 'anti-plane longitudinal' orientation, the crack path appears to be little influenced by the osteons (encircled by the white arrows). (b) A high magnification image of the region indicated by a white circle showing evidence of uncracked-ligament bridging as a contribution to the toughness (indicated by white arrows). (c) A high magnification micrograph showing crack bridging by collagen fibrils, also for 'anti-plane longitudinal' orientation. (d) A stronger influence of microstructure is evident for the 'transverse' orientation, where cracking ahead of the notch is shown at a Haversian canal, although the actual initiation process is at the notch itself, as evidenced by the presence of precursor cracks (Figure 8d). The insets show the specimen orientation with respect to the direction of the osteons; the black arrows indicate the nominal direction of crack growth. (e) Experimental (bridged) and theoretical (traction-free) load-displacement curves (at fixed crack length) used to assess the compliance to verify the existence (and quantify) the bridging levels involved.

as a leading factor associated with the marked anisotropy in the fracture properties of cortical bone.

Such notions on the mechanisms of toughening in bone and how they vary with orientation are consistent with fracture toughness measurements. Using fatigue precracked bend samples, fracture toughness values of $K_c = 5.33(\pm 0.41)$ MPa$\sqrt{}$m were measured for the transverse orientation, as compared to $2.21(\pm 0.18)$ MPa$\sqrt{}$m for anti-plane longitudinal orientation and $3.53(\pm 0.13)$ MPa$\sqrt{}$m for the in-plane longitudinal orientation.

These observations and measurements can be verified by experiment and theory. The highest toughness is in the 'transverse' orientation where the crack path deflects at 90 degrees to the plane of maximum tensile stress (Figure 11d). Linear-elastic calculations using crack-deflection mechanics (Cotterell and Rice, 1980) suggest that for such an in-plane deviation of the crack path, the stress intensity experienced at the crack tip would be reduced by some 50% compared to that for an undeflected crack, consistent with the toughness being approximately twice as high in this orientation. A smaller toughening effect is seen in the 'in-plane longitudinal' orientation where crack bridging by uncracked ligaments (and collagen fibrils) is apparent (Figure 11b). To verify whether such bridging is effective, measurements of the elastic compliance (inverse stiffness) of the cracked bone were compared to those made where the wake of the crack had subsequently machined out; the latter measurements were also verified by showing that they were identical to the theoretical compliance for a traction-free crack of the same size, using the method of Ritchie et al. (1989). Results for the 'anti-plane longitudinal' orientation are shown in Figure 11e and clearly indicate that the crack in the bone

has a lower compliance than a traction-free crack of identical length. Such results provide strong evidence that cracks in human bone are indeed bridged.

The effect of this bridging on the toughness of bone can be quantified from the difference between the two compliance curves at maximum load, which gives the additional load sustained at the load-line, $P_{br} \sim 1.5$ N, due to the presence of the bridges. This equates to a bridging stress intensity, K_{br}, and hence a contribution to the toughness, of ~ 0.5 MPa$\sqrt{\text{m}}$, i.e., $\frac{1}{4}$ of K_c for this orientation. In comparison, theoretical estimates of uncracked-ligament bridging, based on a limiting crack-opening approach (Shang and Ritchie, 1989), yield values of $K_{br} \sim 0.3$ MPa$\sqrt{\text{m}}$. Such experimental measurements, coupled with the theoretical estimates, strongly suggest that uncracked-ligament bridging provides a finite contribution to the toughening of bone.

These simple materials science experiments clearly show that the local criterion for fracture in human cortical bone is consistent with a *strain-based* criterion. We believe that this is the first direct *experimental* evidence for the validity of the assumption of a strain-based criterion, which has been widely used in theoretical models of the mechanical behavior of bone (Yeh and Keaveny, 2001). In addition, the marked anisotropy in the toughness properties of bone can be rationalized in terms of extrinsic toughening mechanisms induced by specific features at varying dimensions in the microstructure. These results are of interest in that they form the basis of physically-based mechanistic understanding of the fracture and failure of human cortical bone.

4. Conclusions

In this paper, we have shown how novel materials-science experiments can shed light on the mechanisms of fatigue and fracture in small-volume structures associated with silicon MEMS and in biological materials such as human bone. It is clear that the materials scientist and engineer can play a major role in both the 'nano' and 'bio' materials arenas. Indeed, there is a need for both sound engineering data and mechanistic understanding. Perhaps even more important is that for both MEMS and biological implants/devices, physically-based life-prediction analyses are sadly lacking, and this makes the realistic evaluation of the durability and reliability of these components and structures uncertain. It is clear that this represents an ideal future challenge for the materials community.

Acknowledgements

This work was supported by the Director, the Office of Science, Office of Basic Energy Sciences, Division of Materials Sciences and Engineering, of the U.S. Department of Energy under Contract No. DE-AC03-76SF00098 (for studies of silicon), and by National Institutes of Health under Grant No. SR01DE01S633 (for studies on mineralized tissue). Special thanks are due to Drs. John H. Kinney, Roya Maboudian and James S. Stölken for their collaboration with us on these studies.

References

Allameh, S.M., Gally, G., Brown, S. and Soboyejo, S.O. (2000). *Materials Science of MEMS Devices III* (edited by H. Kahn *et al.*), MRS, pp. EE2.3.1-EE2.3.6.

Ashurst, W.R., Yau, C., Carraro, C., Maboudian, R. and Dugger, M.T. (2001). *JMEMS* **10**, 41–49.

Brown, S.B., Van Arsdell, W. and Muhlstein, C.L. (1997). *Proc. Int Solid State Sensors and Actuators Conf. (Transducers '97)* (edited by S. Senturia), IEEE, pp. 591–593.
Burr, D.B. (2002). *Bone* **31**, 8–11.
Campbell, J.P., Venkateswara Rao, K.T. and Ritchie, R.O. (1999). *Metall. Mater. Trans. A* **30A**, 563–577.
Connally, J.A. and Brown, S.B. (1992). *Science* **256**, 1537–1539.
Cotterell, B. and Rice, J.R. (1980). *Int. J. Fract.* **16**, 155–169.
Dauskardt, R.H. (1993). *Acta Metal. Mater.* **41**, 2765–2781.
Fargeix, A. and Ghibaudo, G. (1984). *J. Appl. Phys.* **56**, 589–591.
Griffiths, J.R. and Owen, D.R.J. (1971). *J. Mech. Phys. Solids* **19**, 419–431.
Kahn, H., Ballarini, R., Mullenand, R.L. and Heuer, A.H. (1999a). *Proc. Roy. Soc. A* **455**, 3807–3823.
Kahn, H., Tayebi, N., Ballarini, R., Mullen, R.L. and Heuer, A.H. (1999b). *Transducers '99: 10th Int. Conf. Solid State Sens. & Actuat.*, Elsevier, Oxford, UK, pp. 274–280.
Keyak, J.H. and Rossi, S.A. (2000). *J. Biomech.* **33**, 209–214.
Komai, K., Minoshima, K. and Inoue, S. (1998). *Micros. Tech.* **5**, 30–37.
Lathabai, S., Rödel, J. and Lawn, B.R. (1991). *J. Am. Ceram. Soc.* **74**, 1340–1348.
Lawn, B.R., Hockey, B.J. and Wiederhorn, S.M. (1980). *J. Mater. Sci.* **15**, 12.
Lawn, B.R., Marshall, D.B. and Chantikul, P. (1981). *J. Mater. Sci.* **16**, 1769–1775.
Lotz, J.C., Cheal, E.J. and Hayes, W.C. (1991). *J. Biomech. Eng.* **113**, 353–360.
Muhlstein, C.L., Brown, S.B. and Ritchie, R.O. (2001a). *JMEMS* **10**, 593–600.
Muhlstein, C.L., Brown, S.B. and Ritchie, R.O. (2001b). *Sensors and Actuators A* **94**, 177–188.
Muhlstein, C.L., Howe, R.T. and Ritchie, R.O. (2004). *Mech. Mater.* **36**, 13–33.
Muhlstein, C.L., Stach, E.A. and Ritchie, R.O. (2002a). *Appl. Phys. Lett.* **80**, 1532–1534.
Muhlstein, C.M., Stach, E.A. and Ritchie, R.O. (2002b). *Acta Mater.* **50**, 3579–3595.
Nalla, R.K., Kinney, J.H. and Ritchie, R.O. (2003). *J. Biomed. Mater. Res.* **67**, 484–495.
Nalla, R.K., Stölken, J.S., Kinney, J.H. and Ritchie, R.O. (2004). *J. Biomech.*, in review.
Parsamian, G.P. and Norman, T.L. (2001). *J. Mater. Sci.: Mater. Med.* **12**, 779–783.
Rho, J.Y., Kuhn-Spearing, L. and Zioupos, P. (1998). *Med. Eng. Phys.* **20**, 92–102.
Ritchie, R.O. (1999). *Int. J. Fract.* **100**, 55–83.
Ritchie, R.O., Knott, J.F. and Rice, J.R. (1973). *J. Mech. Phys. Solids* **21**, 395–410.
Ritchie, R.O., Server, W.L. and Wullaert, R.A. (1979). *Metall. Trans. A* **10A**, 1557–1570.
Ritchie, R.O., Yu, W. and Bucci, R.J. (1989). *Eng. Fract. Mech.* **32**, 361–377.
Shang, J.K. and Ritchie, R.O. (1989). *Metall. Trans. A* **20A**, 897–908.
Suresh, S. (1998). *Fatigue of Materials*, 2nd edn., Cambridge University Press, Cambridge, UK.
Van Arsdell, W.W. and Brown, S.B. (1999). *JMEMS* **8**, 319–327.
Vashishth, D., Tanner, K.E. and Bonfield, W. (2000). *J. Biomech.* **33**, 1169–1174.
Wang, X., Bank, R.A., Tekoppele, J.M. and Agrawal, C.M. (2001). *J. Orthopaed. Res.* **19**, 1021–1026.
Weiner, S. and Wagner, H.D. (1998). *Ann. Rev. Mater. Sci.* **28**, 271–298.
Yeh, O.C. and Keaveny, T.M. (2001). *J. Orthopaed. Res.* **19**, 1001–1007.
Yeni, Y.N. and Norman, T.L. (2000). *J. Biomed. Mater. Res.* **51**, 504–509.
Yeni, Y.N. and Fyhrie, D.P. (2001). *Proc Bioeng. Conf. BED 50*, ASME, New York, pp. 293–294.
Zioupos, P., Currey, J.D., Mirza, M.S. and Barton, D.C. (1995). *Philos. Trans. R. Soc. Lond. B. Biol. Sci.* **347**, 383–396.